

AI Poincaré: Machine Learning Conservation Laws from Trajectories

Ziming Liu and Max Tegmark

Department of Physics, Massachusetts Institute of Technology, Cambridge, USA

(Dated: April 27, 2021)

We present *AI Poincaré*, a machine learning algorithm for auto-discovering conserved quantities using trajectory data from unknown dynamical systems. We test it on five Hamiltonian systems, including the gravitational 3-body problem, and find that it discovers not only all exactly conserved quantities, but also periodic orbits, phase transitions and breakdown timescales for approximate conservation laws.

INTRODUCTION

While machine learning has contributed to many physics advances, such as improving the speed or quality of numerical simulations, laboratory experiments and astronomical observations [1–7], a more ambitious goal is to design intelligent machines to make new scientific discoveries such as physical symmetries [8–12] and formulas via symbolic regression [13–17]. In this spirit, the goal of the present paper is to auto-discover conservation laws from trajectories of dynamical systems.

Physicists have traditionally derived conservation laws in a *model-driven* way, such as when Poincaré proved [18] that the 3D gravitational 3-body problem has only 10 conserved quantities. In contrast, this paper aims to discover conservation laws in a *data-driven* way, using only observed trajectory data as input while treating the underlying dynamical equations as unknown.

To the best of our knowledge, [11, 12] have pursued the goal closest to ours, but with an orthogonal approach detecting symmetry with an auto-encoder and Siamese neural networks respectively, requiring hand-crafted features precluding full automation, and testing on relatively simple examples. Other work linking conservation laws and machine learning [9, 19–21] focus on embedding physical inductive biases (such as the existence of a Hamiltonian or Lagrangian) into machine learning, but not the other way around to apply machine learning for auto-discovery of conservation laws.

Our ambitious goal of automating conservation law discovery is enabled by recent machine-learning progress [22] for sampling *manifolds*, which are intimately related to dynamical systems as summarized in Table I: viewing each state as a point in a phase space \mathbb{R}^N , the topological closure of the set of all states on a trajectory form a manifold $\mathcal{M} \subset \mathbb{R}^N$. Each conservation law removes one degree of freedom from the dynamical system and one dimension from \mathcal{M} , so the number of conserved quantities is simply N minus the dimensionality of \mathcal{M} [23]. The local tangent space of \mathcal{M} represents all local displacements allowed by conservation laws, while the space perpendicular to the tangent space is spanned by gradients of conserved quantities.

We introduce our notation and AI Poincaré algorithm in the Methods section. In the Results section, we ap-

TABLE I: Manifold/dynamical system correspondence

Manifold	Dynamical System
Dimensionality reduction	Conservation law
Tangent space	Conserved quantity isosurface
Orthogonal space	Gradients of conserved quantities

ply AI Poincaré to five Hamiltonian systems to test its ability to discover conserved quantities (numerically and symbolically), periodic orbits, phase transitions, and conservation breakdown timescales.

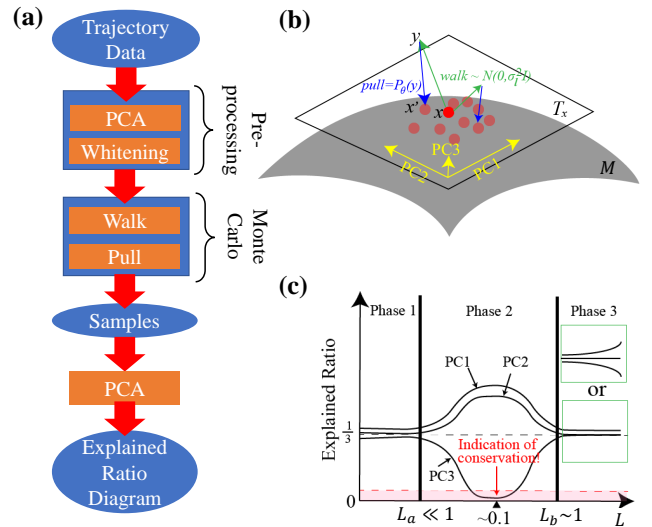


FIG. 1: The AI Poincaré algorithm: (a) overall workflow, (b) walk-pull Monte Carlo module, (c) typical explained ratio diagram, with Phase 2 revealing conserved quantities.

METHOD

Problem and notation: Consider a dynamical system whose state vector $\mathbf{x} \in \mathbb{R}^N$ evolves according to an ordinary differential equation $\frac{d\mathbf{x}}{dt} = f(\mathbf{x}, t)$ for some smooth function f . In physics, dynamical systems can often be written with \mathbf{x} as the concatenation of vectors of generalized coordinates \mathbf{q} and momenta \mathbf{p} and N is even. For the special case of *Hamiltonian systems*, important in classical mechanics [23], there exists a Hamiltonian

function $H_0(\mathbf{q}, \mathbf{p})$ such that

$$\frac{d\mathbf{p}^{(i)}}{dt} = -\frac{\partial H_0}{\partial \mathbf{q}^{(i)}}, \quad \frac{d\mathbf{q}^{(i)}}{dt} = \frac{\partial H_0}{\partial \mathbf{p}^{(i)}} \quad (i = 1, \dots, k). \quad (1)$$

Conservation laws are important in physics, common examples including conservation of energy (H_0), momentum, angular momentum, Runge-Lenz vector, magnetic moment, *etc.* We express a set of independent conservation laws as $H_j[\mathbf{x}(t)] = h_j$, $j = 0, \dots, n - 1$, valid exactly or approximately. Each conservation law can be understood as a mathematical constraint that slices the original n -dimensional phase space into a family of iso-surfaces. We define the *permissible state manifold* (PSM) as $\mathcal{M} \equiv \{\mathbf{x} \in \mathbb{R}^N | H_j(\mathbf{x}) = h_j\}$, *i.e.*, as the set of states allowed by all conservation laws. It is clear that $\dim(\mathcal{M}) = N - n$ [23], since each conservation law removes one degree of freedom from the system. In practice, however, only trajectory data rather than the full PSM is observed, which motivates us to define the *trajectory set* as $\mathcal{S} = \{\mathbf{x}(t) | t \geq 0\}$. If the system is ergodic, \mathcal{S} will be everywhere dense in \mathcal{M} so that \mathcal{M} is the closure $\bar{\mathcal{S}}$ of \mathcal{S} , implying the identity $n = N - \dim(\bar{\mathcal{S}})$. This generalizes even beyond traditional physics contexts: for example, if \mathbf{x} contains the pixel colors in a grey-scale video, then the color of a pixel that always remains black is a conserved quantity.

AI Poincaré We present a machine learning algorithm, *AI Poincaré*, that uses \mathcal{S} to compute an estimator \hat{s} of the dimensionality $s \equiv \dim(\bar{\mathcal{S}})$, thus obtaining an estimator $n_{\text{eff}} \equiv N - \hat{s}$ of n . If $n_{\text{eff}} > 0$, it suggests the existence of n_{eff} hitherto undiscovered conservation laws. If $n_{\text{eff}} = 0$, the system is not Hamiltonian since it lacks even a single conserved quantity H_0 .

Although manifold learning is an active field and has developed powerful tools to explore and visualize the latent structure of low-dimensional submanifolds of high-dimensional spaces [24–29], they either focus on performance on downstream tasks (*e.g.*, image/video generation) where the dimensionality is a user-specified input parameter, or perform not as well as the proposed method here on our task. The supplemental material compares the performance with the PCA, auto-encoder and fractal methods. If we had perfect noiseless samples forming a dense set \mathcal{S} in \mathcal{M} , then we could simply determine the manifold dimensionality s as the rank (number of nonzero eigenvalues) of the covariance matrix of the samples in an infinitesimal environment of a random sample, where the manifold can be approximated by a hyperplane. In practice, we cannot probe infinitesimal scales because we have only a finite number of points, yet we must avoid large scales where manifold curvature is important; our method handles these complications by treating dimensionality s as a renormalized quantity that is a function of length scale L .

AI Poincaré consists of three modules as illustrated in FIG. 1 (a): (1) Pre-processing (prewhitening and op-

tional dimensionality reduction), (2) local Monte Carlo sampling of \mathcal{M} and (3) linear dimensionality estimation from these samples using PCA explained ratios. The prewhitening performs an affine transformation such that the points in \mathcal{S} have zero mean and covariance matrix \mathbf{I} , the identity matrix. If any eigenvalues of the original covariance matrix vanish, then the corresponding eigenvectors \mathbf{e}_i define linear conserved quantities $H_i(\mathbf{x}) = \mathbf{e}_i \cdot \mathbf{x}$, and we remove these dimensions before proceeding. The supplementary material gives further technical details of the preprocessing module.

Our module for Monte Carlo sampling the manifold benefits from the neural empirical Bayes technique in the machine learning literature [22]. It consists of two steps, as illustrated in FIG. 1 (b):

- Walk step $\mathbf{x} \mapsto \mathbf{y}$: perturb a state vector $\mathbf{x} \in \mathcal{S}$ by adding isotropic Gaussian noise \mathbf{n} with zero mean and covariance $L\mathbf{I}$.
- Pull step $\mathbf{y} \mapsto \mathbf{x}'$: pull the “noisy” state \mathbf{y} back toward the manifold. We do this by training the parameters $\boldsymbol{\theta}$ of a feedforward neural network implementing a “pull function” $P_{\boldsymbol{\theta}}$ mapping \mathbb{R}^N to \mathbb{R}^N , minimizing the loss function

$$Loss(\boldsymbol{\theta}) = \frac{1}{N_s} \sum_{i=1}^{N_s} |P_{\boldsymbol{\theta}}(\mathbf{y}_i) - \mathbf{x}_i|_2^2, \quad (2)$$

Where N_s is the number of samples. Since the best the neural network can do is learn to orthogonally project points back onto the manifold, the pulled-back points $\mathbf{x}'_i \equiv P_{\boldsymbol{\theta}}(\mathbf{y}_i)$ characterize the local tangent space when L is appropriately chosen [22].

The Supplementary Material provides further intuition and illustrations regarding how the preprocessing walk/pull steps work.

Explained Ratio Diagram The output of the AI Poincaré algorithm is the *explained ratio diagram* (ERD), showing the fraction of variance explained by each principal component (its eigenvalue divided by the eigenvalue sum) as a function of noise length scale L , revealing the dimensionality of \mathcal{M} and hence the number of conserved quantities. A typical ERD is shown in FIG. 1 (c), revealing three phases separated by phase transitions at $L_a \ll 1$ and $L_b \sim 1$. In the intermediate phase $L_a \lesssim L \lesssim L_b$, some principal component(s) drop near zero and are identified as sub-manifold structure (conservation laws). In the other two phases, all explained ratios are $\sim 1/n$ because the Monte Carlo sample covariance matrix $\sim \mathbf{I}$: on large scales because almost the whole (prewhitened) manifold is sampled and on small scales because of roughly isotropic noise.

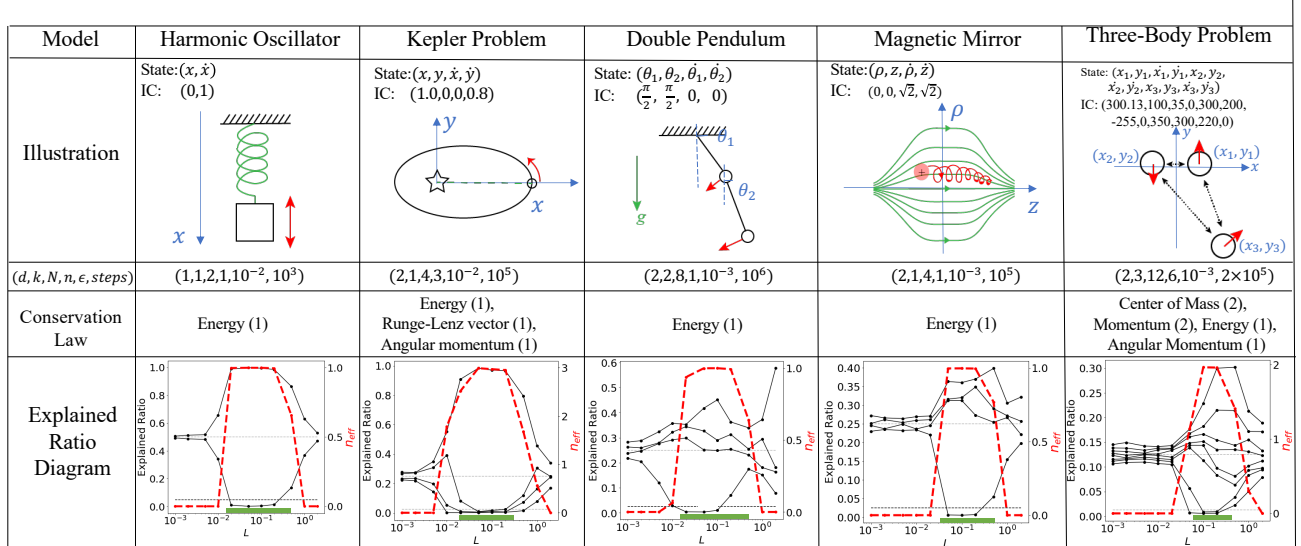


FIG. 2: Five Hamiltonian systems used to test AI Poincaré: Harmonic oscillator, Kepler problem, double pendulum, magnetic mirror and three-body problem. d is the dimensionality of the Euclidean space, k the number of bodies, $N \equiv 2kd$ is the phase space dimensionality, and n the ground truth number of conservation laws. In the bottom panel, the red dashed curve shows the effective number of conserved quantities n_{eff} defined by equation (3), and the green region on the L -axis shows L -range that gets n_{eff} correct (after rounding to the nearest integer). The horizontal dashed lines shows $1/N$ and $0.1/N$; any principal component explaining less than a fraction $0.1/N$ of the total variance at any L is considered evidence for a conservation law.

System	Conserved quantity	Formula found?
Harmonic Oscillator	$H = \frac{1}{2}(x^2 + \dot{x}^2)$	Yes
Kepler Problem	$H = \frac{1}{2}(\dot{x}^2 + \dot{y}^2) - \frac{1}{\sqrt{x^2 + y^2}}$	Yes
	$L_{\text{angular}} = x\dot{y} - y\dot{x}$	Yes
	$A = \arg(L(-\dot{y}, \dot{x}) - \hat{r})$	No
Double Pendulum	(Small angle) $H_s = 10\theta_1^2 + 5\theta_2^2 + \theta_1^2 + \frac{1}{2}\theta_2^2 + \theta_1\theta_2$	Yes
	(Large angle) $H_l = -20\cos\theta_1 - 10\cos\theta_2 + \theta_1^2 + \frac{1}{2}\theta_2^2 + \theta_1\theta_2\cos(\theta_1 - \theta_2)$	No
Magnetic Mirror	$H = \frac{1}{2}(\dot{\rho}^2 + \dot{z}^2) + \frac{1}{2}(\rho^2 + \frac{1}{5}z^2 + \rho^2 z^2)$	Yes
Three Body Problem	$H = \sum_{i=1}^3 \frac{m}{2}(\dot{x}_i^2 + \dot{y}_i^2) - m^2(\frac{1}{r_{12}} + \frac{1}{r_{13}} + \frac{1}{r_{23}}), \quad m = 5 \times 10^6$	No
	$x_c = \frac{1}{3}(x_1 + x_2 + x_3)$	Yes
	$y_c = \frac{1}{3}(y_1 + y_2 + y_3)$	Yes
	$\dot{x}_c = \frac{1}{3}(\dot{x}_1 + \dot{x}_2 + \dot{x}_3)$	Yes
	$\dot{y}_c = \frac{1}{3}(\dot{y}_1 + \dot{y}_2 + \dot{y}_3)$	Yes
	$L_{\text{angular}} = \sum_{i=1}^3 x_i \dot{y}_i - y_i \dot{x}_i$	Yes

TABLE II: Symbolic formulas for 10 of the 13 conservation laws were discovered using AI Feynman.

RESULTS

Numerical experiments We test AI Poincaré on trajectories from five well-studied Hamiltonian systems: the 1D harmonic oscillator, the 2D Kepler problem, the double pendulum, the 2D magnetic mirror and the 2D three-body problem, as defined in Table II and illustrated in FIG. 2. We compute trajectories for the five systems with a the 4th-order Runge-Kutta integrator at $N_{step} = \{10^3, 10^5, 10^6, 10^5, 2 \times 10^5\}$ timesteps of size $\epsilon = \{10^{-2}, 10^{-2}, 10^{-3}, 10^{-3}, 10^{-3}\}$, using the initial conditions listed in FIG. 2. We parametrize the pull function P_θ as a feedforward neural network with two hidden layers containing 256 neurons each, and train it for each L using the ADAM optimizer [30] with learning rate 10^{-3} for 5,000 steps. We repeat the walk+pull Monte Carlo process jumping 10^4 times from the trajectory midpoint.

Basic results The resulting explained ratios (FIG. 2, bottom) show a consistent valley around $L = 0.1$ revealing the number of conserved quantities. The number of conservation laws discovered by AI Poincaré is seen to agree with the ground truth (TABLE II) for all five systems if we simply define the criterion for conservation law discovery as an explained ratio that is an order of magnitude below baseline ($0.1/N$; dashed black line in the figure). For the three-body problem, the first four conservation laws are linear and hence discovered already in our preprocessing step. As shown in the supplemental material, these results are robust to changing the starting point for the walk+pull process, and outperform the PCA, autoencoder and fractal methods for dimensionality estimation.

Symbolic formula discovery TABLE II (right column) shows that we can not only auto-discover that a conservation law exists, but in many cases also a symbolic formula for it: we did this by applying the AI Feynman symbolic regression algorithm [16, 17] to our trajectory data. Since any function of a conserved quantity is also conserved, we require some form of “gauge fixing” to make the symbolic regression problem well posed. Here we simply require states on two chosen trajectories to have conserved value 1 and 2; this approach can undoubtedly be greatly improved, *e.g.*, by requiring that gradient directions match those of our pull function.

Phase transition discovery We will now explore how AI Poincaré can auto-discover not only *exact* conservation laws as above, but also *approximate* ones, revealing physically interesting phase transitions. There are many reasonable ways of defining an *effective number of conserved quantities* n_{eff} as a smooth function of the explained ratios w_i . We want each explained ratio w_i to contribute 1 for small w_i and 0 for $w_i \gtrsim 1/N$, so here we make the simple choice

$$n_{\text{eff}} \equiv \max_L n_{\text{eff}}(L), \quad n_{\text{eff}}(L) \equiv \sum_{i=1}^N c[\pi N w_i(L)], \quad (3)$$

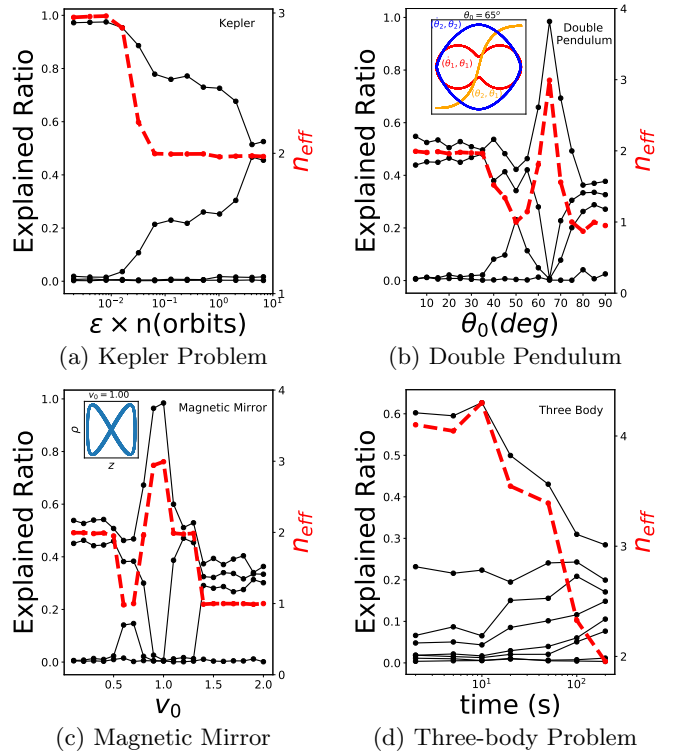


FIG. 3: AI Poincaré detection of phase transitions, approximate conserved quantities and periodic orbits, using n_{eff} as an order parameter.

where $c(x) \equiv \cos x$ if $x < \pi/2$, vanishing otherwise. This is seen to agree well with our threshold criterion (FIG. 2, bottom). Below we fix $L = 0.1$ instead of maximizing over it to save computation time. Let us view n_{eff} as an *order parameter* of the dynamical system and consider phase transitions in the parameter space spanned by timescale, initial conditions and Hamiltonian modifications.

For the **Kepler problem**, we generalize the inverse square force to the form $F \propto r^{-(2+\epsilon)}$, $|\epsilon| \ll 1$. This causes the previously conserved Runge-Lenz vector (the major axis direction) to precess by an angle $\sim \epsilon$ per orbit [31], so that its approximate conservation breaks down after $\sim \epsilon^{-1}$ orbits. AI Poincaré is seen to auto-discover this phase transition (FIG. 3a) without using any of the aforementioned physics knowledge.

The **double pendulum** is known to have a regular phase at low energy and a chaotic phase at high energy [32], both with $n_{\text{eff}} = 1$ (conserving only total energy). We change the initial conditions to $\theta_1 = \theta_2 = \theta_0$ and plot the dependence of n_{eff} on θ_0 (FIG. 3b), which is seen to reveal two additional phases. (1) An interesting periodic orbit ($n_{\text{eff}} = 3$) is discovered at $\theta_0 \approx 65^\circ$ (see inset figure), by adjusting initial conditions to maximize n_{eff} . (2) For small θ_0 , the small angle approximation allows the system to be accurately linearized and decoupled into two non-interacting normal modes, whose energies

are separately conserved ($n_{\text{eff}} = 2$).

The **Magnetic mirror** is also known to have a regular low-energy phase and a chaotic high-energy phase [33], both with $n_{\text{eff}} = 1$ (conserving only energy). We change the initial conditions to $\dot{\rho} = \dot{z} = v_0/\sqrt{2}$ and the dependence of n_{eff} on v_0 in FIG. 3c is seen to reveal two additional phases. (1) An interesting periodic orbit ($n_{\text{eff}} = 3$) is discovered at $v_0 \approx 1.0$ (see inset figure). (2) At low energy (small v_0), the magnetic moment is an adiabatic invariant, so $n_{\text{eff}} = 2$.

For the three-body problem, we consider initial conditions akin to a tight binary star pair orbiting a more distant star. FIG. 3d reveals that the local energy and angular momentum of the tight binary are approximately conserved initially, increasing n_{eff} by 2, until tidal interactions with the distant star eventually cause this conservation to break down.

CONCLUSIONS

We have presented *AI Poincaré*, a machine learning algorithm for auto-discovering conserved quantities using trajectory data from unknown dynamical systems. Tests on five Hamiltonian systems showed that it auto-discovered not only the number of conserved quantities, but also periodic orbits, phase transitions and breakdown timescales for approximate conservation laws. AI Poincaré is universal in the sense that it does not require any domain knowledge or even a physical model of how the trajectories were produced. It may therefore be interesting to apply it to raw experimental data, for example measured neuron voltages in *C. elegans*. Another promising future direction is improved discovery of symbolic formulas for the discovered conserved quantities by transferring learned geometric information from AI Poincaré to AI Feynman, *e.g.*, by requiring that symbolic gradient directions match those of our learned pull function.

Acknowledgements We thank Qihao Cheng, Artan Sheshmani and Huichao Song for helpful discussions and the Center for Brains, Minds, and Machines (CBMM) for hospitality. This work was supported by The Casey and Family Foundation, the Foundational Questions Institute, the Rothberg Family Fund for Cognitive Science and IAIFI through NSF grant PHY-2019786.

Supplementary material

Appendix A: Preprocessing details

As mentioned in the main text, our AI Poincaré method begins with a pre-processing step consisting of

prewhitening and optional dimensionality reduction. The prewhitening performs an affine transformation such that the points in \mathcal{S} obtain zero mean and covariance matrix \mathbf{I} , the identity matrix. If any eigenvalues of the original covariance matrix vanish, then the corresponding eigenvectors \mathbf{e}_i define linear conserved quantities $H_i(\mathbf{x}) = \mathbf{e}_i \cdot \mathbf{x}$, and we remove these dimensions before proceeding. In practice, we consider an eigenvalue λ to vanish if

$$|\lambda_i| < \epsilon_p \max_i \lambda_i, \quad (\text{A1})$$

where $\epsilon_p = 0.001$ is the only tunable hyperparameter in AI Poincaré aside from those associated with neural network architecture and training. The absolute value is needed in equation (A1) because, although a covariance matrix is by definition positive semidefinite, numerical errors in the eigenvalue computation can produce small negative numbers. Below, we provide motivation and further details for the prewhitening and dimensionality reduction.

1. Why prewhitening helps

As mentioned in the main text, the dimensionality of the manifold \mathcal{M} can be read off from the explained-ratio diagram at an intermediate range of length scales L that is sandwiched between two phase transitions at $L_a \ll 1$ and $L_b \sim 1$. In the other two phases, all explained ratios are $\sim 1/n$ because the Monte Carlo sample covariance matrix $\sim \mathbf{I}$: on large scales because almost the whole (prewhitened) manifold is sampled and on small scales because of roughly isotropic noise. Thus L_a is determined by the noise lengthscale, and L_b is determined roughly by the curvature radii of the manifold. If a manifold is highly anisotropic, it can have quite different curvature radii in different directions, replacing a sharp easy-to-spot transition at L_b by a very slowly rising curve. This suggests that prewhitening can help by making the manifold more isotropic, thus pushing its the different curvature scales closer together, far from the noise scale, widening the interval $[L_a, L_b]$ from which we try to measure the manifold's dimensionality.

This intuition is supported by the numerical experiment results shown in FIG. 4. Here we test AI Poincaré without the pre-processing module, using a toy dataset where the manifold is an ellipse with semimajor axis $a = 1$ and semiminor axis b , *i.e.*, with eccentricity $e = \sqrt{1 - b^2}$. To this, we add Gaussian noise with standard deviation ΔL . The top panel shows that $L_a \sim \Delta L$ as expected, *i.e.*, that the leftmost phase transition occurs at the noise scale. The bottom panel shows why prewhitening helps: when the ellipse is more anisotropic, the second phase transition becomes less prominent and therefore harder to detect. In the limit where $b \rightarrow 0$, the ellipse would collapse toward a line and thus contribute to one rather than two principal components.

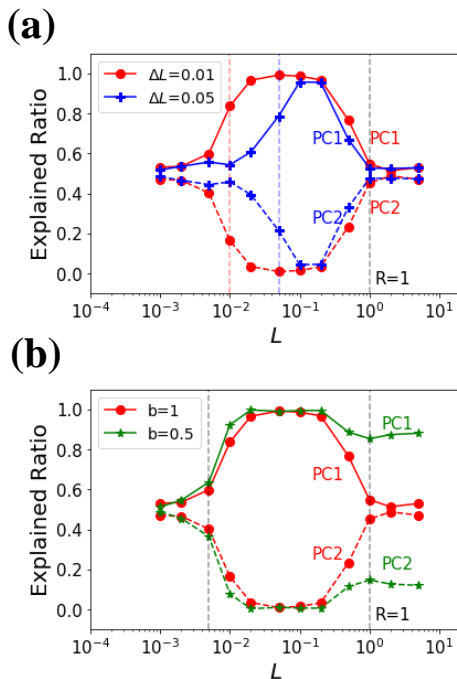


FIG. 4: AI Poincaré applied to ellipse with noise scale ΔL and principal axes 1 and b , showing that (a) the location of the first phase transition is determined by the noise scale ΔL and (b) the sharpness of the second phase transition is determined by the axis ratio of the ellipse, motivating our prewhitening procedure.

2. Robustness to dimensionality reduction and noise

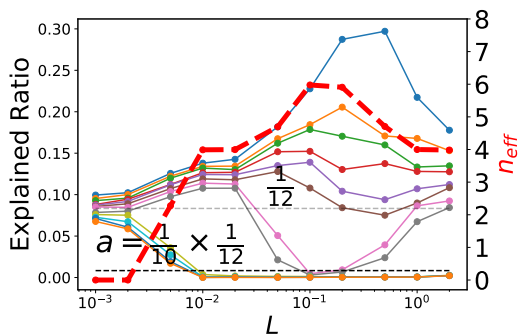


FIG. 5: Explained ratio diagram for the three body problem when linear conserved quantities are not removed in preprocessing (see text), showing that AI Poincaré nonetheless discovers all $n = 6$ conserved quantities at $L = 0.1, 0.2$ and all $n = 4$ linear conserved quantities even at $L = 1, 2$.

In this subsection, we demonstrate that although dimensionality reduction is useful and simplifies subsequent calculations, our basic AI Poincaré method is robust

enough that it can work even without it. FIG. 5 shows the three-body problem reanalyzed without removing the four principal components corresponding to linear conserved quantities, correctly discovering all $n_{\text{eff}} \approx 6$ conserved quantities at $L \in [0.1, 0.2]$ and asymptoting to $n_{\text{eff}} \approx 4$ at $L \gtrsim 1$, since four linear conserved quantities survive even at large scales. To avoid division by near-zero in the prewhitening process, we modified it for this experiment so that each principal component was divided not by its standard deviation $\lambda_i^{1/2}$ but by $\lambda_i^{1/2} + \epsilon_n$, where $\epsilon_n = 0.001$.

Let us also briefly comment on the robustness of our method to noise. FIG. 6 illustrates the effect of adding independent random noise to all data points before the prewhitening step. As long as the added to all data points is drawn from a distribution with the same variance σ^2 , the noise covariance matrix $\sigma^2 \mathbf{I}$ commutes with the data covariance matrix, so the effect of the noise is simply to add σ^2 to all eigenvalues. We see that this 3-body problem example allows the four linearly conserved quantities (corresponding to the four smallest eigenvalues) to be easily recovered as long as the noise level $\sigma \lesssim 0.01$.

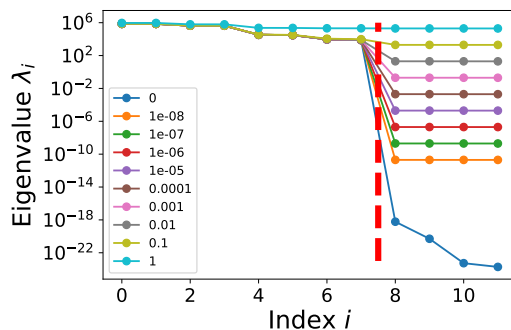


FIG. 6: Three body problem: noise dependence of PCA eigenvalues.

Appendix B: Monte Carlo Module

In this section, we provide additional technical details about our implementation of AI Poincaré's Monte Carlo module. Our method takes input N_s points on a trajectory, which is split into two by using the odd/even points for training/testing, respectively, and used to train the walk/pull network as described in the main text. Consequently, the pull network learns about the manifold in a *global* sense, from the full trajectory. FIG. 7 illustrates this walk/pull step on a circle. Intuitively, the pull network learns to pull points to the closest point on the manifold, which makes the combined walk and pull step approximate a random walk on the manifold.

At inference time (after training this pull network), we randomly select *one* starting point (by default the mid-

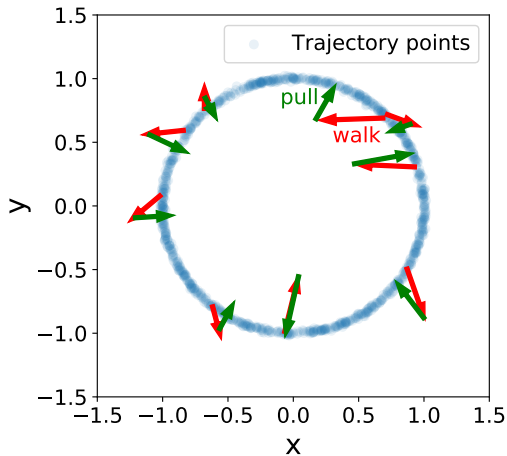


FIG. 7: Monte Carlo module illustration: walk and pull steps on a circle. The walk step randomly perturbs points off the manifold (the circle), after which the pull network projects them back toward the manifold.

point of the trajectory) and perform 10^3 walk/pull steps to obtain samples, the principal components of which are *local* in the sense that they depend on the starting point. We do this merely to save computer time, since the starting point can be any point on the manifold, and n_{eff} can be averaged for many starting points.

To test the stability of AI Poincaré against different choices of starting point, we randomly select 100 points on the trajectory for testing. At each point \mathbf{x} and at each noise scale L , we implement 1,000 walk and pull steps to obtain 1,000 samples, and then apply PCA to obtain explained ratios and calculate $n_{\text{eff}}(\mathbf{x}, L)$. For each point \mathbf{x} , we select the L that maximizes n_{eff} , *i.e.*, we define $n_{\text{eff}}(\mathbf{x}) \equiv \max_L n_{\text{eff}}(\mathbf{x}, L)$. FIG. 8 shows the histogram of $n_{\text{eff}}(\mathbf{x})$ for the 100 random starting points, revealing that the standard deviation of n_{eff} is quite small. If we round $n_{\text{eff}}(\mathbf{x})$ to the closest integer, we obtain the correct number of conserved quantities 100 out of 100 times for all five of our physical systems.

Appendix C: Method comparisons

In this section, we compare the performance of AI Poincaré with the following three other methods for estimating the dimensionality s of a state-space manifold \mathcal{M} by analyzing the point set $\mathcal{S} \subset \mathcal{M}$.

1. **PCA:** A popular method for dimensionality estimation is to perform a principal component analysis of the covariance matrix of the points and estimate the dimensionality as the number of large eigenvalues.

2. **Auto-encoder:** An auto-encoder is simply a non-linear generalization of PCA, where the input vector $\mathbf{x} \in \mathbb{R}^N$ is transformed nonlinearly (but smoothly) to $\mathbf{y} \in \mathbb{R}^s$ and then transformed back to $\mathbf{x}' \in \mathbb{R}^N$ in such a way that average reconstruction error $|\mathbf{x}' - \mathbf{x}|^2$ is minimized. The dimensionality can then be estimated as the smallest s that results in accurate reconstruction.

3. **Fractal Method:** If a manifold has inherent dimensionality s , one would expect the number of point pairs separated by less than L to scale as $N \propto L^s$ for small L , so the dimensionality (even if fractal, *i.e.*, non-integer) can be estimated as the slope of $\log N$ as a function of $\log L$.

FIG. 9 shows the results of applying AI Poincaré and these three methods to each of our five physics examples. Unsurprisingly, PCA performs the worst: because it is simply a *linear* autoencoder, it can only discover linear conserved quantities (that confine the data to a hyper-plane), and therefore discovers only the four linearly conserved quantities for the 3-body problem. A trivial example where PCA fails is a circle: it has two equally large principal components even though it is a one-dimensional manifold. Note that, in contrast, AI Poincaré uses PCA for dimensionality estimation *locally*, not globally as we have done here.

For the fractal method, we manually identify an intermediate range of scales where the slope $d \log N / d \log L$ is roughly constant and estimate dimensionality from that. We do this because, as described in the main text, we expect the effective dimensionality to depend on scale, approaching N on small scales (because of noise) and large scales (because of manifold curvature). FIG. 9 shows that, after some manual tuning of these ranges, we were able to get the correct dimensionality for four of the five cases. The fractal method is slower than AI Poincaré because the number of pairs scales as the square of the number of points, so we used a random subset 10^3 random points for this figure.

For the auto-encoder, FIG. 9 shows that we are able to obtain the correct manifold dimensionalities (and hence the correct number of conserved quantities) if we manually tune the threshold defining “accurate” as 10^{-3} . Unfortunately, the figure also shows that the inferred dimensionalities depend strongly on the choice of this threshold, and that this choice is far from obvious in cases such as that of the double pendulum: the reconstruction error curves lack sharp and clear-cut phase transitions that can guide this threshold choice. This may be at least in part due to topological problems, since topologically non-trivial manifolds may require extra dimensions to auto-encode with a continuous mapping. In contrast, every single one of the five AI Poincaré n_{eff} curves is seen to have an obvious flat plateau, so the simple criterion $n_{\text{eff}} \equiv \max_L n_{\text{eff}}(L)$ works every time. Another advan-

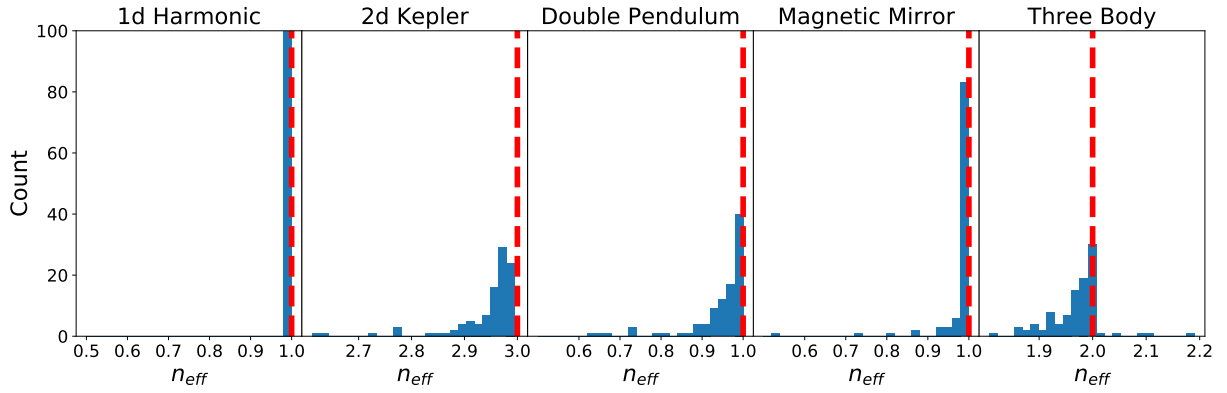


FIG. 8: Stability tests of AI Poincaré for the results in FIG. 2. The predictions by AI Poincaré (blue) have relatively small deviations from ground truth (dashed red line), so rounding to the nearest integer provides excellent error correction.

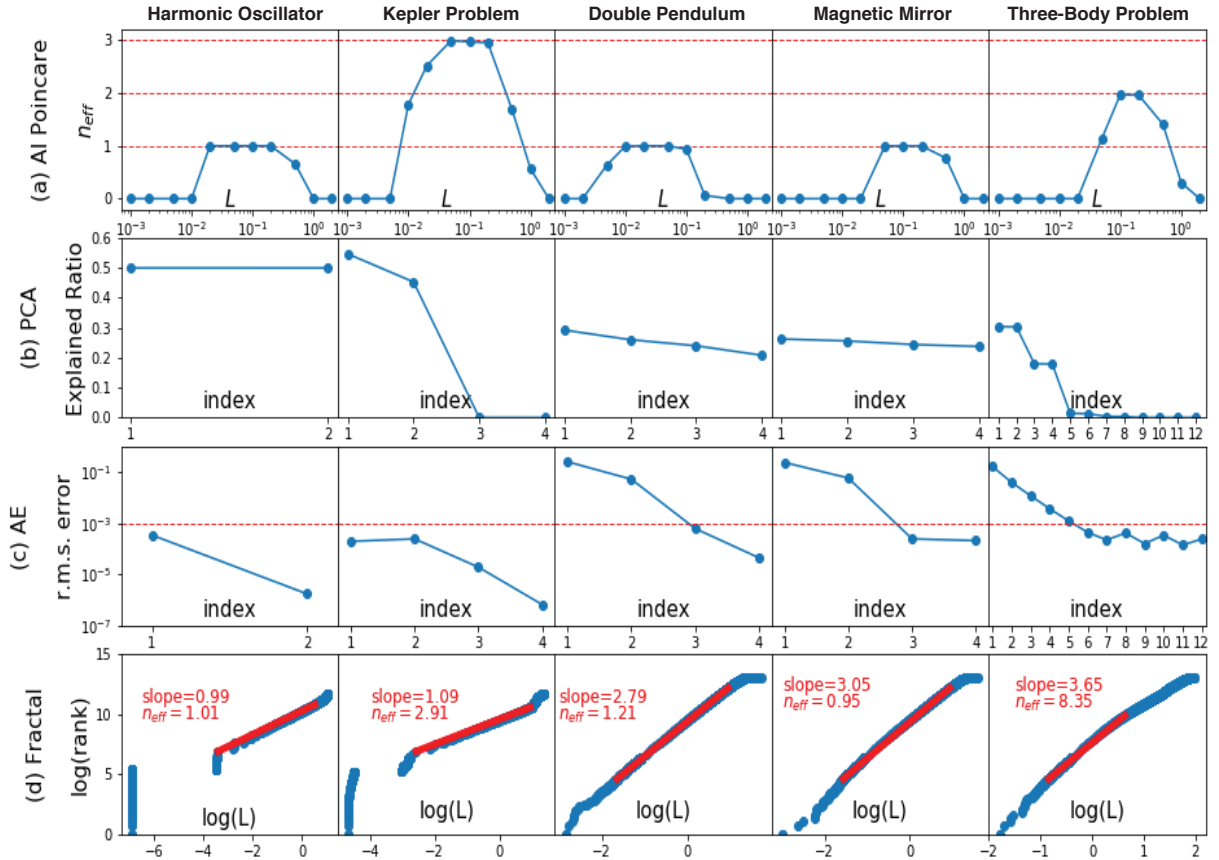


FIG. 9: Performance of the (a) AI Poincaré, (b) PCA, (c) Auto-encoder (c) Auto-encoder and (d) Fractal methods for conserved quantity discovery. The ground truth n_{eff} is 1 (Harmonic Oscillator), 3 (Kepler Problem), 1 (Double Pendulum), 1 (Magnetic Mirror) and 6 (Three Body Problem; 2 after linear dimensionality reduction).

tage of AI Poincaré over the other methods is that it can measure dimensionality also *locally*, at each part of the manifold separately.

Appendix D: Does AI Poincaré overfit?

To test whether AI Poincaré has a tendency to overfit, we train the pull network using only odd-numbered trajectory points, while holding back the even-numbered

TABLE III: Training Loss/Testing Loss

Model	$L = 0.01$	$L = 0.1$	$L = 1$
Harmonic	.000073/.000072	.0033/.0038	0.42/0.40
Kepler	.000059/.000057	.00074/.00083	0.41/0.39
Double Pendulum	.000099/.000097	.0076/.0071	0.44/0.44
Magnetic Mirror	.00012/.00011	.0068/.0066	0.48/0.51
Three Body	.000099/.00011	.0068/.0065	0.46/0.42

points for testing, and tabulated the AI Poincaré training loss and testing loss for all five of our physical systems at various length scales. As can be seen in Table III, this reveals no evidence of overfitting where testing loss is systematically larger than training loss.

Appendix E: Does AI Feynman overfit?

As described in the main text, AI Feynman is trained to discover a formula that is as constant as possible (=1 and 2, respectively) on two different trajectories. To test for overfitting, we quantify how constant the discovered formula is by computing its mean and standard deviation along a third trajectory not seen at training time. The results in Table IV indicate no evidence of overfitting, *i.e.*, that the test error is systematically larger than the training error.

Our criterion for whether AI Feynman succeeds in finding the correct formula is that the discovered formula is mathematically identical to the ground truth formula up to 3% variations in fitted numerical coefficients. For example, the ground truth is that the harmonic oscillator has energy $H = \frac{1}{2}(x^2 + p^2)$. Since $H' \equiv aH + b = \frac{1}{2}ax^2 + \frac{1}{2}ap^2 + b$ is also conserved, we consider the discovered equation as correct if H' has the functional form $H' = cx^2 + dp^2 + e$ and $|\frac{c}{a} - 1| < 3\%$.

-
- [1] E. van Nieuwenburg, Y.-H. Liu, and S. Huber, Learning phase transitions by confusion, *Nature Physics* **13**, 435–439 (2017).
- [2] Y. D. Hezaveh, L. P. L'evasseur, and P. J. Marshall, Fast automated analysis of strong gravitational lenses with convolutional neural networks, *Nature* **548**, 555–557 (2017).
- [3] N. Sun, J. Yi, P. Zhang, H. Shen, and H. Zhai, Deep learning topological invariants of band insulators, *Physical Review B* **98**, 10.1103/physrevb.98.085402 (2018).
- [4] P. Baldi, P. Sadowski, and D. Whiteson, *Nature communications* **5**, 4308 (2014).
- [5] L.-G. Pang, K. Zhou, N. Su, H. Petersen, H. Stöcker, and X.-N. Wang, *Nature communications* **9**, 210 (2018).
- [6] M. Raissi, P. Perdikaris, and G. Karniadakis, Physics-informed neural networks: A deep learning framework for solving forward and inverse problems involving nonlinear partial differential equations, *Journal of Computational Physics* **378**, 686 (2019).
- [7] M. S. Albergo, G. Kanwar, and P. E. Shanahan, Flow-based generative models for markov chain monte carlo in lattice field theory, *Phys. Rev. D* **100**, 034515 (2019).
- [8] A. Decelle, V. Martin-Mayor, and B. Seoane, Learning a local symmetry with neural networks, *Phys. Rev. E* **100**, 050102 (2019).
- [9] M. Mattheakis, P. Protopapas, D. Sondak, M. D. Giovanni, and E. Kaxiras, Physical symmetries embedded in neural networks (2019), arXiv:1904.08991 [physics.comp-ph].
- [10] R. Bondesan and A. Lamacraft, Learning symmetries of classical integrable systems, in *ICML 2019 Workshop on Theoretical Physics for Deep Learning* (2019) arXiv:1906.04645 [physics.comp-ph].
- [11] Y. ichi Mototake, Interpretable conservation law estimation by deriving the symmetries of dynamics from trained deep neural networks, in *Machine Learning and the Physical Sciences Workshop at the 33rd Conference on Neural Information Processing Systems (NeurIPS)* (2019) arXiv:2001.00111 [physics.data-an].
- [12] S. J. Wetzel, R. G. Melko, J. Scott, M. Panju, and V. Ganesh, Discovering symmetry invariants and conserved quantities by interpreting siamese neural networks, *Phys. Rev. Research* **2**, 033499 (2020).
- [13] S. Kim, P. Y. Lu, S. Mukherjee, M. Gilbert, L. Jing, V. Čeperić, and M. Soljačić, Integration of neural network-based symbolic regression in deep learning for scientific discovery (2019), arXiv:1912.04825 [cs.LG].
- [14] P. Y. Lu, S. Kim, and M. Soljačić, Extracting interpretable physical parameters from spatiotemporal systems using unsupervised learning (2019), arXiv:1907.06011 [physics.comp-ph].
- [15] M. Cranmer, A. Sanchez-Gonzalez, P. Battaglia, R. Xu, K. Cranmer, D. Spergel, and S. Ho, Discovering symbolic models from deep learning with inductive biases (2020), arXiv:2006.11287 [cs.LG].
- [16] S.-M. Udrescu and M. Tegmark, Ai feynman: A physics-inspired method for symbolic regression, *Science Advances* **6**, 10.1126/sciadv.aay2631 (2020).
- [17] S.-M. Udrescu, A. Tan, J. Feng, O. Neto, T. Wu, and M. Tegmark, Ai feynman 2.0: Pareto-optimal symbolic regression exploiting graph modularity (2020), arXiv:2006.10782 [cs.LG].
- [18] H. Poincaré, *Les méthodes nouvelles de la mécanique céleste*, Gauthier-Villars , 1 (1892-1899).
- [19] M. Cranmer, S. Greydanus, S. Hoyer, P. Battaglia, D. Spergel, and S. Ho, Lagrangian neural networks, *ArXiv abs/2003.04630* (2020).
- [20] S. Greydanus, M. Dzamba, and J. Yosinski, Hamiltonian neural networks, in *NeurIPS* (2019).
- [21] M. Lutter, C. Ritter, and J. Peters, Deep lagrangian networks: Using physics as model prior for deep learning, in *International Conference on Learning Representations* (2019).
- [22] S. Saremi and A. Hyvärinen, Neural empirical bayes, *J. Mach. Learn. Res.* **20**, 181:1 (2019).
- [23] H. Goldstein, *Classical Mechanics* (Addison-Wesley, 1980).
- [24] J. B. Tenenbaum, V. d. Silva, and J. C. Langford, A global geometric framework for nonlinear dimensionality reduction, *Science* **290**, 2319 (2000).
- [25] S. T. Roweis and L. K. Saul, Nonlinear dimensionality

TABLE IV: How empirically conserved are the symbolic conserved quantities found by AI Feynman?

Conserved quantity	Formula found?	Trajectory 1 (training)	Trajectory 2 (training)	Trajectory 3 (testing)
Harmonic: energy	Yes	1.002 ± 0.005	2.001 ± 0.010	1.457 ± 0.003
Kepler: energy	Yes	1.02 ± 0.03	1.97 ± 0.05	1.35 ± 0.04
Kepler: angular momentum	Yes	1.01 ± 0.01	1.98 ± 0.03	1.48 ± 0.02
Kepler: Runge-Lenz vector	No			
Double pendulum ($ \theta_0 \ll 1$): energy	Yes	1.04 ± 0.07	1.97 ± 0.05	1.48 ± 0.06
Double pendulum ($ \theta_0 \sim 1$): energy	No			
Magnetic mirror: energy	Yes	1.02 ± 0.04	2.03 ± 0.05	1.45 ± 0.07
Three-body: energy	No			
Three-body: angular momentum	Yes	1 ± 0.02	2 ± 0.03	1.77 ± 0.02
Three body: x_c	Yes	$1 \pm .00002$	$2 \pm .00005$	$1.354 \pm .00004$
Three body: y_c	Yes	$1 \pm .00004$	$2 \pm .00003$	$1.445 \pm .00003$
Three body: \dot{x}_c	Yes	$1 \pm .00003$	$2 \pm .00002$	$1.327 \pm .00002$
Three body: \dot{x}_y	Yes	$1 \pm .00008$	$2 \pm .00002$	$1.813 \pm .00004$

reduction by locally linear embedding, *Science* **290**, 2323 (2000).

- [26] L. V. D. Maaten and G. E. Hinton, Visualizing data using t-sne, *Journal of Machine Learning Research* **9**, 2579 (2008).
- [27] B. Luo, R. C. Wilson, and E. R. Hancock, Spectral embedding of graphs, *Pattern Recognition* **36**, 2213 (2003).
- [28] D.-Y. Tzeng and R. S. Berns, A review of principal component analysis and its applications to color technology, *Color Research & Application* **30**, 84 (2005).
- [29] M. A. Kramer, Nonlinear principal component analysis using autoassociative neural networks, *AICHE Journal* **37**, 233 (1991).
- [30] D. P. Kingma and J. Ba, Adam: A method for stochastic optimization, *CoRR* **abs/1412.6980** (2015).
- [31] J. D. Wells, When effective theories predict: the inevitability of mercury’s anomalous perihelion precession (2011), arXiv:1106.1568 [physics.hist-ph].
- [32] T. Stachowiak and T. Okada, A numerical analysis of chaos in the double pendulum, *Chaos, Solitons and Fractals* **29**, 417 (2006).
- [33] G. Contopoulos, M. Harsoula, and C. Efthymiopoulos, Analytical study of chaos and applications, *The European Physical Journal Special Topics* **225**, 1053 (2016).